Rapid Communications

Two-dimensional isotropic turbulent inflow conditions for vortex particle method

Sparsh Sharma*
Technical Acoustics, Brandenburg Technical University, Cottbus 03046, Germany

Ennes Sarradj
Technical Acoustics, Technical University-Berlin, Berlin 10857, Germany

(Received 27 July 2018; published 19 February 2019)

The unsteady loading on an airfoil due to the inflow turbulence is the primary source of broadband noise in turbomachinery, which makes the modeling of the inflow conditions a crucial task. This Rapid Communication presents an advanced method to model isotropic turbulent inflow conditions for a two-dimensional vortex particle method. The method relies on the classical view of turbulence as a superposition of random vortices convected with the mean flow. The fluctuating velocity is formulated using the scalar potential given by a convolution product which furnishes a solenoidal velocity field. The system is then optimized stochastically to create a realistic turbulence field based on a target energy spectra using an evolutionary optimization algorithm.

DOI: 10.1103/PhysRevFluids.4.022701

I. INTRODUCTION

Acoustic radiation from a body immersed in a turbulent flow field, popularly known as Leading Edge noise, is a widely studied topic in Computational Aeroacoustics. The early studies [1–3] show the use of frequency domain analysis in which the incoming disturbance is modeled as a series of harmonic gusts by analyzing the fields Fourier transform. Studies based on this method have accounted for the effects of thickness, camber, and angle of attack, but were mainly used for relatively low frequencies. As the frequency increases, the spatial and temporal resolution requirements make these numerical methods more difficult to apply [4]. Another prevalent method in use is the time-domain analysis [5–7] which uses a set of discrete vortices to realize the turbulent inflow. However, these studies have not considered the statistical modeling of the inflow due to which the stochastic nature of the disturbance was missing. In more recent papers, Glegg [8] used a time-domain method where the statistical nature of the disturbance was modeled using discrete vortices. Both methods, frequency domain and time domain, have their advantages and limitations which are presented by Grace [9]. She concluded that the time-domain analysis has an advantage over the frequency domain, primarily due to the ability to realize the turbulent inflow with the desired statistical properties.

On the other hand, it is way more challenging to model the inflow conditions using a set of discrete vortices [10], since the parameters which control the size and the strength of these vortices are unknown. These inflow conditions can be imposed by methods which are considerably expensive like those based on proper orthogonal decomposition which requires appropriate direct numerical simulations [11] or experimental data [12] to obtain the energetic modes. Different methods are available to synthesize a turbulent signal without involving the solution to Navier-Stokes equations,

*sparsh.sharma@b-tu.de

and one such way is by superimposing a white noise signal over the mean flow. Chapman [13], Benzi [14], and Elhmaidi [15] used a similar method to realize a two-dimensional synthetic turbulent inflow using point vortices. Esler [16] studied the behavior of a finite number of point vortices and examined the possibility of replacing a turbulent flow with a collection of point vortices. However, there is a problem with approximating the vorticity with point vortices (delta functions), i.e., infinite spikes, which introduces an associated singularity in the streamfunction and velocity fields. This singularity appears when the distance to the point vortex becomes very small.

The main objectives of this Rapid Communication are (1) to overcome this difficulty by replacing the point vortices with the shape function vortices with the details of their implementation, and (2) to optimize these shape function vortices in order to match a realistic two-dimensional (2D) von Kármán energy spectrum. It is shown that the synthesized inflow disturbance satisfies the divergence-free condition and matches the statistics of the desired energy spectra. Section II A presents the kinematics of the vortex particles and the governing equations involved in the Lagrangian frame of reference. The singularity associated with the point vortices as well as its elimination is discussed in Sec. II B followed by the synthesis of the turbulent inflow in Sec. III.

II. VORTEX METHOD

A. Governing equation and the point vortices

Two-dimensional ideal flows are ruled by the Euler equation that, in terms of the $\omega\hat{z} = \boldsymbol{\nabla} \times \mathbf{u}$ (where $\hat{z}$ indicates the perpendicular direction to the xy plane of the flow), reads

$$\frac{\partial \omega}{\partial t} + \mathbf{u}\cdot\boldsymbol{\nabla}\omega = 0, \tag{1}$$

expressing the conservation of vorticity along fluid-element paths. The velocity and the vorticity field are described with the aid of a single scalar streamfunction ψ. Writing the velocity in terms of the streamfunction, $\mathbf{u} = \nabla^{\perp}\psi = (u_1 = \partial\psi/\partial y, u_2 = -\partial\psi/\partial x)^T$, the vorticity is given by

$$\omega = -\Delta\psi, \tag{2}$$

where Δ is the Laplacian operator. The single streamfunction ψ unifies the streamfunctions for each constituent of the flow field: ψ_ω the vorticity of the flow field and the solid body rotation, ψ_γ the vortex sheet distribution on the boundary (body), and ψ_∞ corresponding to the velocity field at infinity,

$$\psi = \psi_\omega + \psi_\gamma + \psi_\infty. \tag{3}$$

Applying the Poincaré identity to each component of the streamfunction ψ in Eq. (3) after combining it with Eq. (2) yields [17]

$$\psi(\mathbf{r}, t) = \underbrace{\int \omega(\mathbf{r}', t)\mathcal{G}(\boldsymbol{r}, \boldsymbol{r}')d\mathbf{r}'}_{\psi_\omega} + \underbrace{\int \left[\left(\frac{\partial(\psi_o - \psi_i)}{\partial n}(\boldsymbol{r}')\mathcal{G}(\boldsymbol{r}, \boldsymbol{r}')\right) - \left((\psi_o - \psi_i)(\boldsymbol{r}')\frac{\partial \mathcal{G}}{\partial \mathbf{n}}(\boldsymbol{r}, \boldsymbol{r}')\right)\right]d\boldsymbol{r}'}_{\psi_\gamma} + \psi_\infty, \tag{4}$$

where $\mathcal{G}(\boldsymbol{r}, \boldsymbol{r}') = 1/(2\pi)\log(|\boldsymbol{r} - \boldsymbol{r}'|)$ is the Green's function of the Laplacian operator Δ, $\boldsymbol{r} = (x, y)$ is a point in the flow field, and $\boldsymbol{r}'$ is the location of the vortex. Equation (4) can be expressed in terms of singularity distributions on the boundary of the domain for which the source distribution and the vortex sheet are defined as

$$\sigma = \psi_o - \psi_i \quad \text{and} \quad \gamma = \frac{\partial \psi_o}{\partial n} - \frac{\partial \psi_i}{\partial n}, \tag{5}$$

respectively. The subscripts o and i represent the area outside the body and the area inside the body, respectively, in the domain. Therefore, the velocity can be expressed in terms of ω as [18,19]

$$\mathbf{u}_\omega(\boldsymbol{r},t) = \nabla^\perp \int \mathcal{G}(\boldsymbol{r},\boldsymbol{r}')\omega(\boldsymbol{r}',t)d\boldsymbol{r}', \tag{6}$$

$$\mathbf{u}_\gamma(\boldsymbol{r},t) = \nabla^\perp \int \left[\gamma(\boldsymbol{r}')\mathcal{G}(\boldsymbol{r},\boldsymbol{r}') - \sigma(\boldsymbol{r}')\frac{\partial \mathcal{G}}{\partial \mathbf{n}}(\boldsymbol{r},\boldsymbol{r}')\right]d\boldsymbol{r}'. \tag{7}$$

The discretized vorticity field is expressed as the sum of the vorticities of the N vortex particles, in which the initial circulation Γ is concentrated, in the following way:

$$\omega(\boldsymbol{r},t) = \sum_{n=1}^{N} \Gamma_n \delta[\boldsymbol{r} - \boldsymbol{r}_n(t)], \tag{8}$$

where $n \in \{1,\ldots,N\}$ is an index to denote each individual vortex. Vorticity is created continuously at the fluid-solid interface as a consequence of continuously satisfying the surface velocity boundary conditions. These conditions are enforced at the boundary elements (panels), which are the discretized surface into N panels of a certain length and enforces the no-slip and no-penetration boundary conditions at the center point of each panel. The domain is discretized into computational nodes, interpreted as either sources, doublets, vortex particles, or the combination of two or all [20]. The surface (sheet) circulation computed by the boundary element method is then released into the flow at each time step as new circulation-carrying particles (vortices).

B. Point vortex singularity and Gaussian wave shape vortices

The resulting velocity field [Eq. (6)] induced by the point vortices raises no problem when used as the singularity distribution on the domain boundaries and/or as the circulation carrier at each timestep. However, Esler and Ashbee [16], and Kuvshinov and Schep [21] showed, in their work on point vortices to realize a white noise signal, that there exists a problem when approximating the vorticity with delta functions (point vortices), i.e., infinite spikes, which is an associated singularity in the streamfunction and velocity field. This singularity appears when the distance to the point vortex becomes very small, $|r - r'| \to 0$: both streamfunction and velocity become very large; the first blows up logarithmically fast and the other like r^{-1}. This is quite problematic in the evaluation of the sums. It therefore becomes necessary to eliminate the "spiky" representation of the vorticity. In this Rapid Communication, a method based on the shape function vortices is adopted to handle these infinite spikes which was first proposed by Jarrin [22], which was later on developed by Sescu and Hixon [23] who showed that this shape function signal satisfies the convecting equations based on the mean flow, which means that scalar potential is convected by the mean flow. The shape function vortices have a finite core which eliminates the associated singularity. The shape function can either be a Gaussian wave or a Mexican hat wavelet or a Morlet wavelet, or a combination of two or all. To build these representations, it is thus assumed that each of the finite-core vortices is associated with a localized shape function, $\psi = f(r)$, that is radially symmetric about the center of the vortex, that decays as we move away from the center, and whose integral over the entire plane is unity. For the current study, the shape function considered for the vortices is the Gaussian wave which is given by

$$\psi(\boldsymbol{r},t) = \gamma\varrho^{-1/2}e^{-[3\varrho r)]^2}, \tag{9}$$

where the right-hand side is a transcendental function, called the shape function (a spatiotemporal polynomial), with γ as the directional strength of the vortex, ϱ controls the size of the vortex [radius of the vortex core, $R = 1/\sqrt{(\varrho)}$], and r is the position of the vortex in the computational domain.

Although it is known that replacing a turbulent flow with a collection of the discrete vortices is an idealized simplification, it sheds light on the possibility of generating a statistically optimized

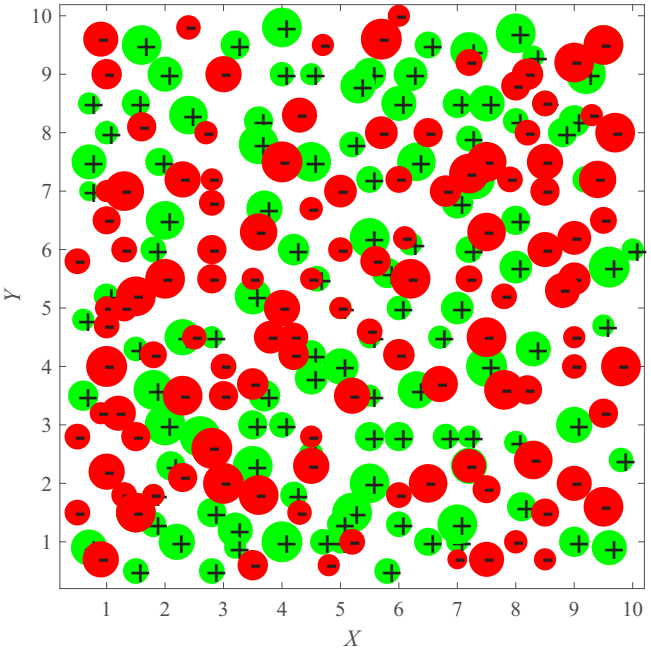

FIG. 1. Distributions of the vortices are indicated by disks with area proportional to the vortex intensity; red symbols indicate negative (clockwise flow) and green symbols indicate positive (counterclockwise flow) circulation, respectively.

turbulent inflow in the time-domain analysis. Since the method is based on an unbounded domain contrary to the synthetic eddy modeling [22] which requires the definition of a precise volume (area for 2D) containing all the turbulent structures, a finite domain of interest is defined and named as *vortex window*. The vortices are randomly distributed in this two-dimensional finite space, as shown in Fig. 1, and are convected along with the mean flow. A general form of the scalar potential, ψ_{turb}, for such a space can be written as

$$\psi_{\text{turb}}(r,t) = \sqrt{\frac{A_{\text{inflow}}}{N}} \sum_{n=1}^{N} \epsilon_n \psi_n \left(\frac{|r-r'|}{L_b}, \frac{t-t'}{\tau_b} \right), \tag{10}$$

where A_{inflow} is the area of the vortices window and N is the total number of vortices. $(A_{\text{inflow}}/N)^{(1/2)}$ indicates the average distance between two adjacent vortices inside the vortices window. ϵ_n is a random sign switch taking the value of -1 or 1 to account for the vortex rotation, ψ_n represents a dimensionless shape function for each individual vortex. r' is the spatial and t' is the temporal location of the vortex. L_b and τ_b denotes the turbulent length and timescales, respectively. Sescu and Hixon [23] also showed that Eqs. (9) and (10) satisfy the Euler equations and therefore genuinely remove the possibility of causing pressure fluctuations from the synthetic vortices.

III. SYNTHESIS OF 2D TURBULENCE

A. Controlling parameters

The next objective of the present study is to realize a realistic turbulent velocity field from the shape function vortices. As turbulence is, by its very nature, stochastic, modeling it using a set of discrete vortices requires few constraints to regulate them to employ the stochasticity. A total of six constraint parameters, listed in Table I, are introduced to control and optimize the overall

TABLE I. Parameters controlling the turbulence statistics.

Parameters	Definition	Values
N	Number of the vortices in the vortex window	100 (fixed)
A_{inflow}	Area of the vortex window	[2(chord length)]^2
$R_{\max}$	Upper limits for the vortex size (radius)	0.5
$R_{\min}$	Lower limits for the vortex size (radius)	0.1
$\gamma_{\max}$	Upper limits for eddy strength	0.01
$\gamma_{\min}$	Lower limits for eddy strength	−0.01

distribution of random vortices to replicate a target energy spectra,von Kármán energy spectra, for a homogeneous isotropic two-dimensional turbulence. Using Eqs. (9) and (10), a Gaussian profile scalar potential can be written as

$$\psi_{\text{turb}}(r,t) = \sqrt{\frac{A_{\text{inflow}}}{N}} \sum_{n=1}^{N} \epsilon_n \left[\left(\gamma_n \varrho_n^{-1/2} e^{-(3\varrho_n \boldsymbol{r}_n)^2} \right) \right]. \tag{11}$$

The resulting fluctuating velocity field for a new vortex profile is obtained by introducing Eq. (11) into $\mathbf{u} = \nabla^{\perp}\psi$ at (x_0, y_0),

$$u_1(\boldsymbol{r},t) = -18\sqrt{\frac{A_{\text{inflow}}}{N}} \sum_{n=1}^{N} \epsilon_n \left[\left(\gamma_n \varrho_n^{3/2} e^{-9\varrho_n^2 \mathbf{r}_n^2} \right)(y - y_0) \right], \tag{12}$$

$$u_2(\boldsymbol{r},t) = 18\sqrt{\frac{A_{\text{inflow}}}{N}} \sum_{n=1}^{N} \epsilon_n \left[\left(\gamma_n \varrho_n^{3/2} e^{-9\varrho_n^2 \mathbf{r}_n^2} \right)(x - x_0) \right]. \tag{13}$$

The three-dimensional view of the Gaussian vortex is also illustrated in Fig. 2, which shows the magnitude of the velocity as the z axis.

B. Homogeneous and isotropic two-dimensional turbulence

The constrained parameters (listed in Table I) define the scalar potential [Eq. (11)] which is used to calculate the numerical spectra. The study of homogeneous and isotropic turbulence is supported by the use of correlation functions. For a two-dimensional incompressible flow, the two-point two-time correlation tensor of the turbulent velocity $\mathbf{u}$ is defined as $\mathcal{R}_{ij}(\boldsymbol{r},\tau) = \langle u_i(\boldsymbol{r}_1,t_1) u_j(\boldsymbol{r}_2,t_2)\rangle$,

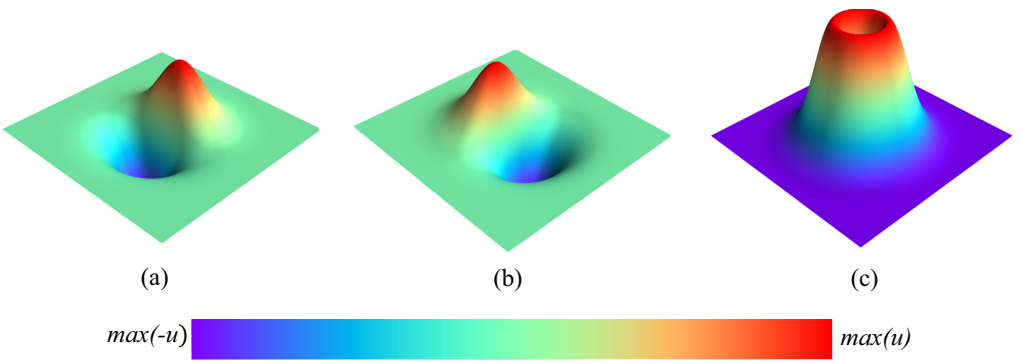

FIG. 2. Three-dimensional view of a Gaussian shape vortex by plotting the magnitude of the (a) u_1, (b) u_2, and (c) $\mathbf{u}$ velocity as the z axis.

where $\langle\cdot\rangle$ denotes the ensemble average, $\boldsymbol{r} = |\boldsymbol{r}_1 - \boldsymbol{r}_2|$, and $\tau = |t_1 - t_2|$. The velocity field is defined in terms of a scalar field $\psi_{\text{turb}}(\boldsymbol{r}, t)$, which is modeled as a homogenous, isotropic, and stationary Gaussian stochastic process. The correlation of the streamfunction can be written as

$$\mathsf{C}_{ij}(\boldsymbol{r}, \tau) = \left\langle \psi_{\text{turb}\,i}(\boldsymbol{r}_1, t_1)\psi_{\text{turb}\,j}(\boldsymbol{r}_2, t_2)\right\rangle. \tag{14}$$

Careta *et al.* [24] showed that C is related to the radial correlation function $\mathcal{R}$ using $\mathbf{u} = \nabla^{\perp}\psi$ and using the properties of the Bessel functions as

$$\mathcal{R}(r) = \frac{1}{2}\mathcal{R}_{ij}(r, 0) = \frac{1}{4\pi}\int_0^{\infty} k^3\widehat{\mathsf{C}}(k)J_0(kr)dk, \tag{15}$$

where $\widehat{\mathsf{C}}$ is the Fourier transform of the correlation function C, $r = |\mathbf{r}|$, and $k = |\boldsymbol{k}|$. J_0 is the Bessel function of the zeroth order. Correspondingly, $\widehat{\mathsf{C}}$ is related to the energy spectrum $E(k)$ of the turbulence as [25]

$$E(k) = \frac{1}{4\pi}k^3\widehat{\mathsf{C}}(k). \tag{16}$$

Kraichnan [18] showed that the fluctuating velocity field, $\mathbf{u}$, can be expressed as

$$\mathbf{u}(\boldsymbol{r}, t) = \nabla^{\perp}\underbrace{\int \mathcal{G}(\boldsymbol{r}, \boldsymbol{r}')\mathcal{U}(\mathbf{r}', t)d\boldsymbol{r}'}_{\psi_{\text{turb}}}, \tag{17}$$

where $\mathcal{G}$ is a spatial Green's function filter and $\mathcal{U} = (\mathcal{U}_1, \mathcal{U}_2, \mathcal{U}_3)$ is the white noise field which is reduced to a single term, $\mathcal{U} = (0, 0, \mathcal{U}_3)$, for a two-dimensional turbulent flow. Following Dieste and Gabard [25], it is possible to express the streamfunction correlation in terms of the filter as the convolution of the temporal correlation of $\mathcal{U}$, which leads to relating the Fourier transform $\hat{\mathcal{G}}$ of the filter to the energy spectrum:

$$E(k) = \frac{1}{4\pi}k^3\hat{\mathcal{G}}(k)^2. \tag{18}$$

The resulting numerical spectra for fluctuating velocity is obtained by introducing Eq. (11) into Eq. (18) as

$$E(k) = \frac{1}{4\pi}k^3\frac{A_{\text{inflow}}}{N}\sum_{i=1}^{N}\sum_{j=1}^{N}\frac{\gamma_i\gamma_j}{18\sqrt{\varrho_i{}^3\varrho_j{}^3}}\exp\left[-\frac{k^2}{18\left(\varrho_i{}^2 + \varrho_j{}^2\right)}\right]. \tag{19}$$

C. Target spectrum: Homogeneous and isotropic two-dimensional turbulence

The target spectrum $E_{\text{tar}}(k)$ for the numerical spectrum $E(k)$ is the von Kármán energy spectrum for two-dimensional homogeneous isotropic turbulence [26] which is given by

$$E_{\text{tar}}(k) = E^{VK}(k) = \frac{110u_{\text{rms}}^2\Lambda}{27\pi}\frac{\left(\frac{k}{k_c}\right)^4}{\left[1 + \left(\frac{k}{k_c}\right)^2\right]^{17/6}}, \tag{20}$$

$$k_c = \frac{\Gamma\left(\frac{1}{2}\right)\Gamma\left(\frac{5}{6}\right)}{\Lambda\Gamma\left(\frac{1}{3}\right)},$$

where Λ is the integral length scale and Γ is the gamma function. The longitudinal and the transverse spectra can be calculated as

$$E_{11}(k_1) = 2\int \phi_{11}(k)dk_2, \quad E_{22}(k_1) = -k_1\frac{dE_{11}}{dk_1}, \quad \phi_{ij}(k) = \frac{E(k)}{\pi k}\left(\delta_{ij} - \frac{k_ik_j}{k^2}\right), \tag{21}$$

where ϕ_{ij} is the spectral tensor defined as the Fourier transform of the correlation function $\mathcal{R}_{ij}$.

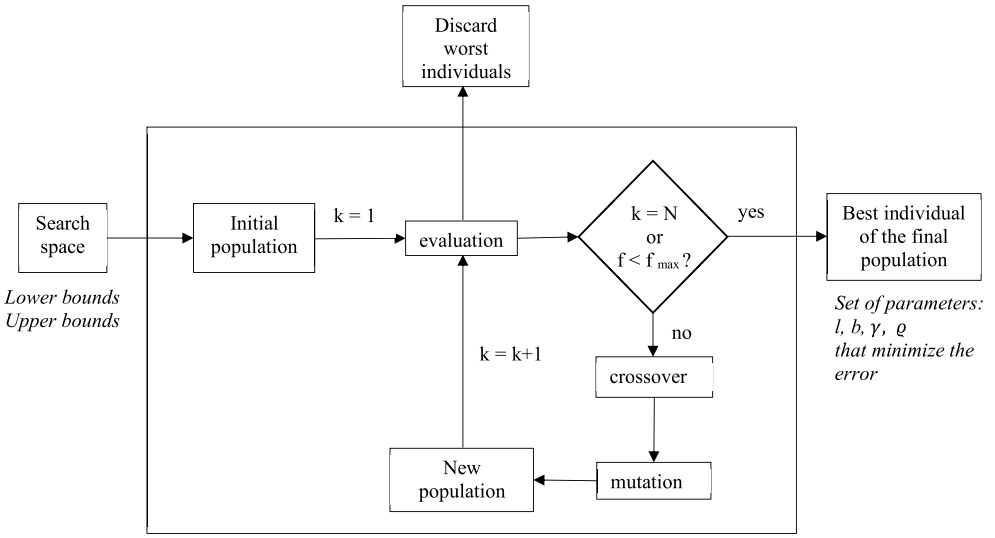

FIG. 3. Scheme of the usage of the genetic algorithm (GA) to optimize the statistics of the newly generated turbulence spectrum to the target one.

In the present study, the vortices window is injected close to the leading edge of the airfoil. $u_{\mathrm{rms}}/u_\infty = 0.02$, which is equivalent to 2.0% turbulence intensity and $\Lambda = 0.04$, which corresponds to the length scale which is nondimensionalized by the chord length of the airfoil, are set as the parameters for the target energy spectrum.

D. Stochastic optimization

The ability of the numerical turbulence to realize the desired statistical properties relies on the optimization of six constrained parameters

$$\mathcal{P} = (N, A_{\mathrm{inflow}}, R_{\mathrm{max}}, R_{\mathrm{min}}, \gamma_{\mathrm{max}}, \gamma_{\mathrm{min}}),$$

where R_{max} and R_{min} are the upper limits and lower limits, respectively, for the vortex size (radius). Similarly, γ_{max} and γ_{min} represent the upper limits and the lower limits, respectively, for the eddy strength. The optimization of these parameters is carried out by defining an error function as

$$\varepsilon(\mathcal{P}) = \left| \log_{10} \frac{\langle E(k) \rangle}{E_{\mathrm{tar}}(k)} \right|. \tag{22}$$

The $E(k)$ spectra, given by Eq. (19), are optimized to $E_{\mathrm{tar}}(k)$ for k values from 1 to 150 by minimizing the error function $\varepsilon(\mathcal{P})$. In previous studies with vortices, Glegg and Devenport [8] and Kim and Haeri [27] used 200 and 300 vortices, respectively, in their work which motivated the current study to begin with 100 vortices for the optimization. The optimization is carried out using an evolution-based optimisation technique, Genetic algorithm (GA) [28]. GA operates on the population of artificial chromosomes. Each chromosome represents a solution to a problem and has a fitness, a real number which is a measure of how good a solution it is to the particular problem.[1] The algorithm takes random values within the identified range for the constrained parameters, and the process is repeated until the best fitting spectra are obtained. The principle is used for the optimization of the newly generated synthetic turbulence as shown in Fig. 3.

[1]The depth discussion of the genetic algorithm is beyond the scope of the current Rapid Communication. The interested readers may refer to Ref. [29].

The first set of simulations is given the population size of 50 for each vortex which go through mutations and crossovers while regenerating to match the objective. Since the objective was not met with a population size of 50, it was decided to keep increasing the population size until the objective is met. For the minimization of the error function given by Eq. (22), the objective was met with a population size of 200. The numerical experiments show that increasing the size of the population from 50 to 200 chromosomes significantly improves the resulting value of the objective function. The further increase in the size of the population (more than 100 chromosomes) does not lead to more accurate results. The subsequent increase in the population size leads only to an increase in computational time without improving the value of the objective function.

The current work presents an efficient method to realize isotropic turbulent inflow conditions. It uses the mathematical background of synthetic turbulence models [23] which comes down to adding modes, rather than solving the Navier-Stokes equation [27]. This makes the method an economical and efficient tool for preliminary estimations in engineering questions.

The target spectra and the optimized one-dimensional spectra for the turbulent inflow is shown in Figs. 4(a) and 4(b). Both the longitudinal and the transverse spectra are in good agreement with the corresponding target ones. In addition, Fig. 4(c) shows a good agreement between the optimized spectra and experimental spectra obtained by Geyer *et al.* [30]. The measurements took place in the small aeroacoustic wind tunnel at the Brandenburg University of Technology, which is an open jet

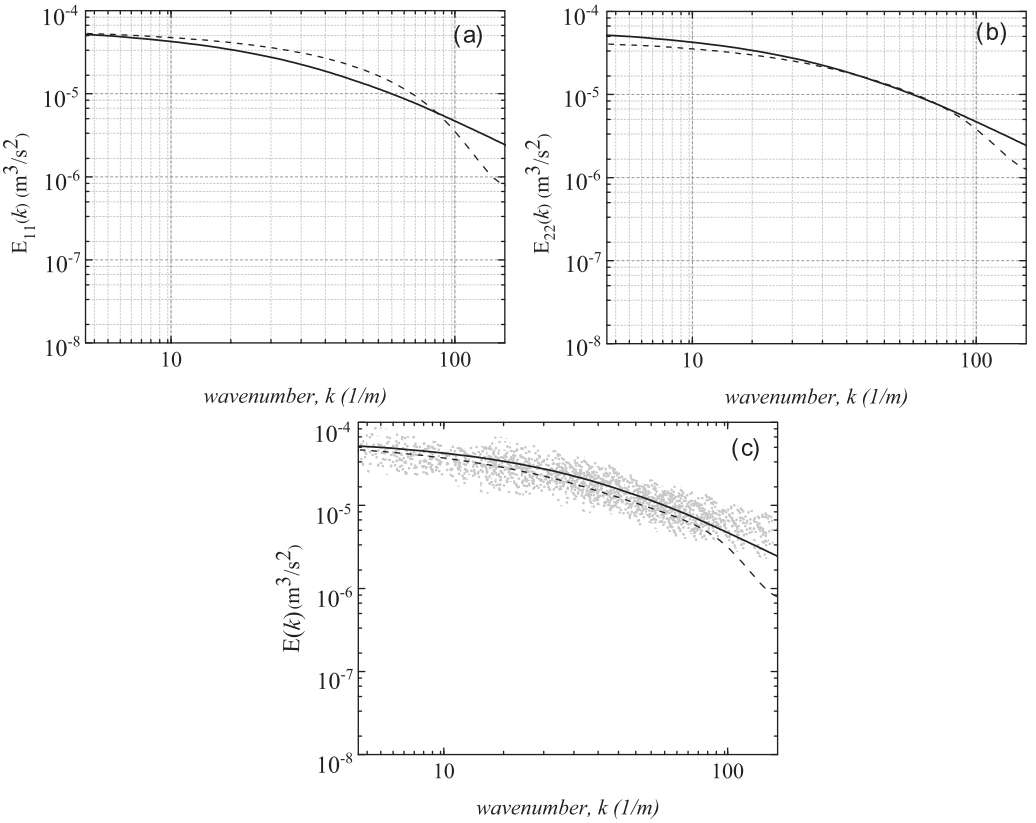

FIG. 4. (a) Longitudinal, (b) transverse von Kármán energy spectra of two-dimensional turbulence with $u_{\text{rms}}/u_\infty = 0.02$ and $\Lambda = 0.04$;—, von Kármán spectrum; - - -, numerical spectra; and (c)—, analytical von Kármán spectrum; - - -, numerical spectra; and experimental spectrum represented by gray dots.

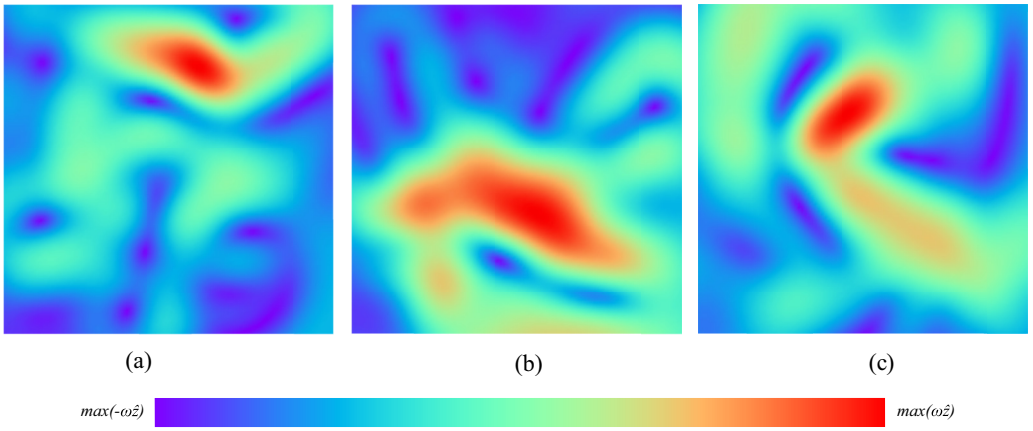

FIG. 5. Contour plot of vorticity field in two dimensions for three random iterations on a grid with spatial resolution of 100 × 100 divisions on the vortex window.

wind tunnel. In the experiments, the parameters of the incident turbulence were determined at 30 measurement positions, randomly distributed in a plane normal to the flow.

IV. CONCLUSION

The objectives of the present Rapid Communication, to overcome the singularity associated with the point vortices and the realization of a statistically matched spectra, are successfully met.

In this Rapid Communication, a scalar potential using a Gaussian wave shape function is derived to construct a stochastic function for the calculation of energy spectra. The Gaussian profile for the vortices eliminates the problem of infinite spikes when the distance to the vortex becomes very small. The derived spectral equations for the energy has the same structure as the spectral equations of Dieste and Gabard [25] and Gea-Aguilera *et al.* [31].

The optimization of the constrained parameters is performed using the genetic algorithm which enhances the randomness in the system because it uses random sampling methods to create generations of random candidate solutions. The vortices are distributed in the model with the average separation between two adjacent vortices less than a fixed critical distance. Figure 5 shows the vorticity field plotted in two dimensions using the optimized constrained parameters for $u_{\mathrm{rms}}/u_{\infty} = 0.02$ and $\Lambda = 0.04$. It shows three different vortex windows with different spatial configurations of vortices but satisfying the same conditions: the divergence-free condition, and the statistics of the desired energy spectrum. The plots give a visual representation of the randomness inhibited by the GA. The grid resolution for the plot is 100 × 100 divisions on the vortex window.

This low-cost methodology aims at providing a realistic and statistically optimized turbulent inflow condition for the broadband noise calculation using a vortex method. It uses a Gaussian shape waveform to construct the spatial filter; however, an advanced scalar potential (vector potential for three-dimensional analysis) can be constructed using different available shape functions.

ACKNOWLEDGMENT

The authors take this opportunity to acknowledge the funding for this work, which was provided by the Graduate Research School (GRS) of BTU within the context of Doctoral Research Assistantship.

[1] P. E. Doak, Acoustic radiation from a turbulent fluid containing foreign bodies, Proc. R. Soc. A **254**, 129 (1960).
[2] I. J. Sharland, Sources of noise in axial flow fans, J. Sound Vib. **1**, 302 (1964).
[3] R. Amiet and W. R. Sears, The aerodynamic noise of small-perturbation subsonic flows, J. Fluid Mech. **44**, 227 (1970).
[4] P. D. Lysakn, D. E. Capone, and M. L. Jonson, Prediction of high frequency gust response with airfoil thickness effects, J. Fluids Struct. **39**, 258 (2013).
[5] M. Gennaretti and G. Bernardini, Novel boundary integral formulation for blade-vortex interaction aerodynamics of helicopter rotors, AIAA J. **45**, 1169 (2007).
[6] D. Rockwell, Vortex-body interactions, Annu. Rev. Fluid Mech. **30**, 199 (1998).
[7] M. Gennaretti, L. Luceri, and L. Morino, A unified boundary integral methodology for aerodynamics and aeroacoustics of rotors, J. Sound Vib. **200**, 467 (1997).
[8] S. A. L. Glegg and W. J. Devenport, Panel methods for airfoils in turbulent flow, J. Sound Vib. **329**, 3709 (2010).
[9] S. M. Grace, Unsteady blade pressure - The BVI model vs. the gust model, in *Proceedings of the 7th AIAA/CEAS Aeroacoustics Conference and Exhibit* (AIAA, Reston, VA, 2001).
[10] S. Sparsh, G. Thomas, and S. Ennes, Time domain boundary element method for the leading edge noise subjected to linear vorticity, *INTER-NOISE and NOISE-CON Congress and Conference Proceedings*, Vol. 258 (Institute of Noise Control Engineering, 2018), pp. 622–631.
[11] P. S. Johansson and H. I. Andersson, Generation of inflow data for inhomogeneous turbulence, Theor. Comput. Fluid Dyn. **18**, 371 (2004).
[12] P. Druault, S. Lardeau, J. P. Bonnet, F. Coiffet, J. Delville, E. Lamballais, J. F. Largeau, and L. Perret, Generation of three-dimensional turbulent inlet conditions for large-eddy simulation, AIAA J. **42**, 447 (2004).
[13] D. M. F. Chapman, Ideal vortex motion in two dimensions: Symmetries and conservation laws, J. Math. Phys. **19**, 1988 (1978).
[14] R. Benzi, S. Succi, and M. Vergassola, The lattice Boltzmann equation: Theory and applications, Phys. Rep. **222**, 145 (1992).
[15] D. Elhmaïdi, A. Provenzale, and A. Babiano, Elementary topology of two-dimensional turbulence from a Lagrangian viewpoint and single-particle dispersion, J. Fluid Mech. **257**, 533 (1993).
[16] J. G. Esler and T. L. Ashbee, Universal statistics of point vortex turbulence, J. Fluid Mech. **779**, 275 (2015).
[17] G.-H. Cottet and P. D. Koumoutsakos, *Vortex methods: Theory and practice* (Cambridge University Press, Cambridge, UK, 2000), p. 313.
[18] R. H. Kraichnan, Diffusion by a random velocity field, Phys. Fluids **13**, 22 (1970).
[19] A. J. Chorin, *Vorticity and turbulence* (Springer, New York, 1994), Vol. 103.
[20] J. Katz and A. Plotkin, *Low Speed Aerodynamics* (Cambridge University Press, Cambridge, 2001), p. 351.
[21] B. N. Kuvshinov and T. J. Schep, Point-vortex approach in two-dimensional turbulence, Plasma Phys. Rep. **42**, 523 (2016).
[22] N. Jarrin, S. Benhamadouche, D. Laurence, and R. Prosser, A synthetic-eddy-method for generating inflow conditions for large-eddy simulations, Int. J. Heat Fluid Flow **27**, 585 (2006).
[23] A. Sescu and R. Hixon, Toward low-noise synthetic turbulent inflow conditions for aeroacoustic calculations, Int. J. Numer. Methods Fluids **73**, 1001 (2013).
[24] A. Careta, F. Sagués, and J. M. Sancho, Stochastic generation of homogeneous isotropic turbulence with well-defined spectra, Phys. Rev. E **48**, 2279 (1993).
[25] M. Dieste and G. Gabard, Random particle methods applied to broadband fan interaction noise, J. Comput. Phys. **231**, 8133 (2012).
[26] C. Bailly and G. Comte-Bellot, *Turbulence*, Experimental Fluid Mechanics (Springer International Publishing, 2015).
[27] J. W. Kim and S. Haeri, An advanced synthetic eddy method for the computation of aerofoil-turbulence interaction noise, J. Comput. Phys. **287**, 1 (2015).

[28] J. H. Holland, *Adaptation in Natural and Artificial Systems: An Introductory Analysis with Applications to Biology, Control, and Artificial Intelligence* (MIT, Cambridge, MA, 2013), pp. 1–6.

[29] J. McCall, Genetic algorithms for modelling and optimisation, J. Comput. Appl. Math. **184**, 205 (2005).

[30] T. F. Geyer, E. Sarradj, and M. Hobracht, Noise generated by a leading edge in anisotropic turbulence, in *Proceedings of the 45th International Congress and Exposition on Noise Control Engineering* (2016), http://pub.dega-akustik.de/IN2016/data/articles/000165.pdf.

[31] F. Gea-Aguilera, J. Gill, and X. Zhang, Synthetic turbulence methods for computational aeroacoustic simulations of leading edge noise, Comput. Fluids **157**, 240 (2017).